Influence of biomass burning plumes on HONO chemistry in eastern China

W. Nie[1,2], A. J. Ding[1,2], Y. N. Xie[1,2], Z. Xu[3], H. Mao[1,2,5], V. Kerminen[4], L. F. Zheng[3,1], X. M. Qi[1,2], X. Q. Yang[1,2], J. N. Sun[1,2], E. Herrmann[1], T. Petäjä[4], M. Kulmala[4] and C. B. Fu[1,2]

[1]Institute for Climate and Global Change Research & School of Atmospheric Sciences, Nanjing University, Nanjing, 210093, China

[2]Colaborative Innovation Center of Climate Change, Jiangsu Province, China

[3] Environment Research Institute, Shandong University, Jinan, China

[4]Division of Atmospheric Sciences, Department of Physics, University of Helsinki, Helsinki, Finland

[5]Department of Chemistry, State University of New York College of Environmental Science and Forestry, Syracuse, New York, USA

Abstract. Nitrous acid (HONO) plays a key role in atmospheric chemistry via influencing the budget of hydroxyl radical (OH). In this study, a two-month measurement period of HONO and related quantities were analyzed during a biomass burning season in 2012 at a suburban site in the western Yangtze River delta, eastern China. An overall high HONO concentration with the mean value of 0.8 ppbv was observed. During biomass burning (BB) periods, both HONO concentration and $HONO/NO_2$ ratio were enhanced significantly compared with non-biomass burning (Non-BB) periods. A correlation analysis showed that the HONO concentration was not associated with potassium (a tracer of BB) in BB plumes, but showed a high correlation with the NO_2 concentration, suggesting a principal role of secondary production rather than direct emissions in elevated HONO concentrations. A further analysis based on comparing the surface area at similar PM levels and $HONO/NO_2$ ratios at similar surface area levels suggested larger specific surface areas and higher NO_2 conversion efficiencies of BB aerosols. A mixed plume of BB and anthropogenic

fossil fuel (FF) emissions was observed on 10 June with even higher HONO concentrations and HONO/NO_2 ratios. The strong HONO production potential (high HONO/NO_2 to $PM_{2.5}$ ratio) was accompanied with a high sulfate concentration in this plume, suggesting a promotion of mixed aerosols to the HONO formation. In summary, our study suggests an important role of BB in atmospheric chemistry by affecting the HONO budget. This can be especially important in eastern China, where agricultural burning plumes are inevitably mixed with urban pollutions.

1. Introduction

Nitrous acid (HONO) is an important constituent in the troposphere due to its role in hydrogen oxides (HO_x) cycling (Platt et al., 1980; Kleffmann, 2007; Hofzumahaus et al., 2009; Elshorbany et al., 2012). The photolysis of HONO provides a daytime source of hydroxyl radical (OH), which controls the daytime oxidation capacity and consequently influences the O_3 chemistry and secondary organic aerosol (SOA) formation. This process appears especially important in the early morning when contributions from other OH sources, like ozone photolysis, are still small (Alicke et al., 2002; Kleffmann et al., 2005; Elshorbany et al., 2010).

The sources of atmospheric HONO, including direct emission from fossil fuel combustion (Kurtenbach et al., 2001) and ground surfaces (Su et al., 2011), homogeneous gas phase reactions and heterogeneous processes on the surface of atmospheric aerosols and ground (Harrison and Collins, 1998; Longfellow et al., 1999; Stutz et al., 2002; VandenBoer et al., 2013), are hitherto not well understood. Among these sources, heterogeneous processes are commonly accepted as the least understood pathway to produce HONO. For example, NO_2 can be converted to HONO on ground (Harrison and Kitto, 1994) or wet surfaces (Finlayson-Pitts et al., 2003), on soot particles (Ammann et al., 1998; Kalberer et al., 1999; Kleffmann and Wiesen, 2005), or on organic substrates (Bröske et al., 2003; Ammann et al., 2005). These processes have been considered as the primary contributor to the nocturnal HONO formation, but they cannot sustain the frequently-observed elevated daytime

HONO concentration levels (Kleffmann, 2007; Sorgel et al., 2011; Li et al., 2012), and the references there in). Recently, several heterogeneous and possibly photo-enhanced processes have been demonstrated that might play an important role in daytime HONO formation (George et al., 2005; Stemmler et al., 2006; Ndour et al., 2008; Nie et al., 2012; Langridge et al., 2009; Bedjanian and El Zein, 2012). However, although these studies have drawn a clearer picture on the HONO chemistry, there are still large knowledge gaps in HONO sources. The principal process contributing to HONO formation in different chemical environments is still under debate.

Biomass burning is a major source of atmospheric aerosol particles (Janhäll et al., 2010) and trace gases (Andreae and Merlet, 2001; Burling et al., 2010), consequently influencing climate and air quality. Recent studies have connected the HONO chemistry to biomass burning via both direct HONO emissions and emissions of soot particles (Roberts et al., 2010; Veres et al., 2010). Although high emission ratios of HONO have been detected in the laboratory fires (Burling et al., 2010; Veres et al., 2010), the mixing ratio of HONO in aged biomass burning plumes is expected to be relatively independent of its direct emissions due to the rapid dilution and other sinks for primary HONO during the atmospheric transport. Soot particles, as one major component in biomass burning plumes, have been demonstrated to be an effective media to convert NO_2 to HONO (Kleffmann et al., 1999; Aumont et al., 1999; Prince et al., 2002; Kleffmann and Wiesen, 2005; Aubin and Abbatt, 2007), especially in the case that aged soot particles can be re-actived in the present of light (Monge et al., 2010) and play a continuous role in the HONO chemistry. These processes may significantly influence the HONO chemistry during a biomass burning period, but their exact roles are rarely demonstrated in the real atmosphere, especially when BB aerosols are mixed with anthropogenic pollutants.

In this study, a two-month measurement campaign was conducted during the intensive biomass burning (BB) period (April to June 2012) at the SORPES station (Stations for Observing Regional Processes of the Earth System) in western Yangtze River delta (YRD) of East China (Ding et al., 2013c). Several HONO-related quantities were

measured, with the aim to investigate the HONO chemistry in YRD, a region undergoing rapid urbanization and industrialization. A special attention was given to the impact of BB plumes and mixed plumes of agricultural burning and fossil fuel (FF) emissions on HONO formation after a long-range transport. In the following, we will first describe the general features related to HONO during the campaign. The differences in HONO formation between the BB events and non-BB events will then be investigated. The influence of mixed plumes of intensive BB and FF emission (Ding et al., 2013b) on HONO formation will be finally discussed.

2. Experimental methodologies

2.1 Filed campaign

The field campaign was conducted from late April to June 2012 at the SORPES "flagship" central site in Xianlin (Ding et al., 2013c). It is a regional background site, located on the top of a hill (118°57'10" E, 32°07'14", 40 m a.s.l.) in the Xianlin campus of Nanjing University and about 20 km east of the suburban Nanjing city (See Fig. 1 in Ding et al., 2013c). A suite of trace gases, aerosols and meteorological quantities were measured, with more detailed descriptions found in Ding et al. (2013b). The present study is focused on HONO and related quantities, including NO_2, $PM_{2.5}$ mass, potassium ions, and particle surface-area size distribution over the size range of 6–800 nm.

2.2 Measurement techniques

The HONO concentration was measured with a Monitor for Aerosols and Gases in Air (MARGA, Metrohm Co.), which includes a wet rotating denuder (WRD) (Spindler et al., 2003; Su et al., 2008; Makkonen et al., 2012) connected to an ion chromatography (IC, Metrohm USA, Inc., Riverview, FL). The time resolution of this measurement is 1 h. There were more than 1500 hourly samples during the campaign. The WRD consists of two concentric glass cylinders whose wall is coated with 10 ppm H_2O_2 solution to absorb HONO and other gases. The liquid sample streams from

WRD are drawn into 25 ml syringes before injecting into the IC system. The residence time of sampling air is about 4.5 s in the sampling tubes and about 0.2 s in WRD.

Other measurement techniques are described briefly as follows. The fine particle mass concentration ($PM_{2.5}$) was continuously measured with a combined technique of light scattering photometry and beta radiation attenuation (Thermo Scientific SHARP Monitor Model 5030). Sulfate and potassium concentrations in $PM_{2.5}$ were measured with the MARGA system (Ding et al., 2013b). NO_2 was converted to NO with a molybdenum oxide (MoO) catalytic converter inside the instrument and measured with a chemiluminescence analyzer (TEI model 42i). We note that the technique of molybdenum converter to measure NO_2 may overestimate its ambient concentrations due to the potential conversion of species other than NO_2 (e.g. PAN) to NO (Xu et al., 2013). NO_y was measured with an externally placed molybdenum converter and a NO analyzer. The SO_2 concentration was measured with a pulsed UV fluorescence analyzer (TEI model 43i). Detailed information can be found in Ding et al. (2013b).

2.3 Sampling artifacts and data correction

The sampling artifacts of HONO measurement with WRD method are mainly caused by the NO_2 conversion on the surface of the sampling tube and WRD (interference 1) and the reaction of NO_2 with S (IV) in the absorption solution in WRD (interference 2) (Spindler et al., 2003; Barnes and Rudziński, 2012). In this study, 10 ppm of H_2O_2 was used as the absorption solution for the MARGA system, which can oxidize the S (IV) very quickly to form H_2SO_4, and thus can avoid the interference 2 induced by the reaction of NO_2 with S (IV) (Genfa et al., 2003). In addition, the formation of H_2SO_4 can acidize the absorption solution, which will reduce the interference 1 in WRD by suppressing the absorption and reaction of NO_2 on the surface of the absorption solution. Therefore, in this study, the interference of HONO measurement should be mainly from the NO_2 conversion on the surface of the sampling tube (part of interference 1). Here, to avoid the possible overestimation aroused by this interference,

we corrected the dataset with the following formula recommended by an inter-comparison study on the HONO measurement between a WRD and a LOPAP system conducted in a similar atmospheric environment in China (Su, 2008):

$HONO_{LOPAP}=0.833*HONO_{WRD}-0.17$

It should be noted that the dataset corrected by this formula is expected to underestimate the HONO concentration because the absorption solution deployed by Su (2008) was Na_2CO_3, which can induce additional interference in WRD (interference 2 and part of interference 1). Given that we probably underestimated the HONO concentrations and overestimated the NO_2 concentration (Xu et al., 2013), the values of $HONO/NO_2$ and $HONO/NO_x$ calculated in section 3 are actually lower limits for these ratios.

Several studies (Appel et al., 1990; Th. Muller, 1999; Genfa et al., 2003) have demonstrated that HONO concentrations measurement by WRD tend to be overestimated mainly during daytime, so we deployed only nighttime data (except the case of 10 June, when the solar radiation was significantly decreased to a very low level (Ding et al., 2013b).) in sections 3.2 and 3.3.

2.4 Calculation of the nocturnal HONO lifetime

There are three major pathways to the loss of HONO during nighttime, including depression on ground surfaces (Path-A), heterogeneous loss on aerosol surfaces (Path-B) and reaction with the OH radical (Path-C) (Li et al., 2012). For Path-A, the HONO lifetime (τ_a) is given by

$$\tau_a = \frac{1}{k_a} = \frac{H}{V_{HONO}}$$

where H is the mixing height (assumed as 100 m) and V_{HONO} is the dry deposition velocity of HONO, assumed to be equal to 0.8 cm s^{-1} (Li et al., 2012). For the loss Path-B, the corresponding lifetime (τ_b) can be written as

$$\tau_b = \frac{1}{k_b} = \frac{1}{\frac{1}{4} * \gamma_{HONO} S_{aerosol} * \overline{v_{HONO}}}$$

where γ_{HONO} is the HONO uptake coefficient on aerosol estimated to be 10^{-3} (Harrison and Collins, 1998; Wong et al., 2011), $S_{aerosol}$ is the aerosol surface during the observation with a mean value of about 1.5×10^3 $\mu m^2/cm^3$ calculated from the particle size distribution, and $\overline{v_{HONO}}$ is the mean molecular velocity of HONO (about 380 m/s). For the loss Path-C, the lifetime (τ_c) is equal to

$$\tau_c = \frac{1}{k_c} = \frac{1}{k * OH}$$

The OH concentration was estimated as 10^6 mol cm^{-3} (Hofzumahaus et al., 2009). $K_{HONO+OH}$ is the reaction rate of HONO and OH. The value of 5.0×10^{-12} cm^3 s^{-1} at 298 K (Sander et al., 2006) was adopted. In these conditions, the overall lifetime, τ, is obtained from the following formula:

$$\frac{1}{\tau} = \frac{1}{\tau_a} + \frac{1}{\tau_b} + \frac{1}{\tau_c}$$

The calculated lifetime of HONO was about 1.5 hours.

3. Result and discussions

3.1 Observation overview

Figure 1 shows the temporal variations of concentrations of HONO, NO_2, $PM_{2.5}$ mass and potassium observed at the Xianlin SORPES central site during the time period of April –June 2012. The average concentration of HONO was 0.76 ± 0.79 ppbv, which is slightly lower than the concentrations measured in a polluted rural site in the Pearl River Delta region (Su et al., 2008) and urban site in Shanghai (Wang et al., 2013), but much higher than those measured in Europe (Acker and Möller, 2007). The HONO concentrations (Fig. 2a) and ratios of HONO to NO_2 (HONO/NO_2) (Fig. 3b) both exhibited distinct diurnal cycles, with a diurnal maximun during night/early

morning and minimum around the noon. The average diurnal amplitude was ~0.8 ppbv for HONO and ~ 0.04 for the HONO/NO_2 ratio.

During the campaign and especially from late May to early June, several BB episodes were observed, revealed by elevated concentrations of $PM_{2.5}$ (exceeding 400 μg m^{-3}) and potassium (exceeding 20 μg m^{-3}) (Fig. 1) (Ding et al., 2013b; Ding et al., 2013c). Interestingly, HONO concentrations were also significantly enhanced during the BB episodes. In order to investigate the relation between BB and HONO chemistry, we compared the HONO concentrations, HONO/NO_2 ratios and HONO/NO_x ratios between the BB and non-BB periods. The samples with potassium concentrations higher than 2 μg m^{-3} and the ratio of potassium to $PM_{2.5}$ larger than 0.02 were defined as BB samples. The samples with potassium concentrations lower than 2 μg m^{-3} and the ratio of potassium to $PM_{2.5}$ smaller than 0.02 were categorized as non-BB samples. On average, all the three parameters of HONO concentration, HONO/NO_2 ratio and HONO/NO_x ratios were significantly higher (about a factor of 2) during BB periods than during other times (Figs. 3d-3f), indicating a positive impact of BB plumes on the ambient mixing ratio of HONO.

The enhanced HONO production in BB plumes would significantly impact the atmospheric oxidation capacity, and in turn influence a series of processes, such as the formation of secondary aerosols (Li et al., 2010; Gonçalves et al., 2012; Elshorbany et al., 2014). In this study, the observed HONO to NO_x ratios (on average 0.028 ± 0.021), especially during the BB periods (on average 0.062 ± 0.031) (see Fig. 3f) were considerably higher than the assumed global averaged value of 0.02 (Elshorbany et al., 2012; Elshorbany et al., 2014), suggesting a potential more important role of HONO chemistry in the YRD, especially during the BB season.

3.2 Influence of BB on HONO formation

3.2.1 Possible influence of direct emission and ground surface

Several laboratory studies have demonstrated BB as an effective HONO source via

direct emissions (Burling et al., 2010; Veres et al., 2010), so HONO might play an important role in atmospheric chemistry over BB source regions. However, HONO is a highly-reactive species that is easily consumed by chemical sinks during its atmospheric transport (the lifetime is about 1.5 hours even in the night time, see section 2.4). In this study, the main BB source area is located in the northern part of Anhui province several hundred kilometers from the SORPES station (Fig. 4). At least several hours were therefore needed before the BB emissions get to our measurement site, which were much longer than the HONO lifetime even in the nighttime. So the contribution of direct emissions to the observed HONO can be considered negligible. To further verify this point, we looked at the relation between HONO and potassium (Fig. 5), as well as between HONO and NO_2 (Fig. 6), during the BB periods. Results showed that HONO was poorly correlated with potassium, a tracer for direct BB emissions, but highly correlated with NO_2, suggesting the key role of chemical conversion rather than direct emissions in causing elevated HONO concentrations. Therefore, the observed high HONO concentrations during the BB periods is expected to be due to either increased precursor concentrations or increased NO_2 to HONO conversion efficiency. As shown in Figs. 1 and 3c, the concentration levels of NO_2 were comparable during the BB and non-BB periods, so the higher HONO level during BB period was probably due in large part to a higher NO_2 conversion potential (HONO/NO_2 ratio).

Both ground and aerosols are effective surfaces for converting NO_2 to HONO. Here, to estimate the possible role of ground surface to the enhanced HONO/NO_2 ratios, we conducted backward Lagrangian dispersion modeling for the air masses arrived the SORPES station using the HYSPLIT following the method developed by Ding et al., (2013a). Considering that the nighttime HONO lifetime is less than 2 hours, we run the models for a 2-hour backward period. Fig. 7a and 7b present the "footprint" retroplumes, which represents the distribution of probability or residence time of the simulated air masses in their last two-hour transport time prior to arrival at measurement site (Ding et al., 2013a). As shown in Fig. 7, the "footprint" for BB and

Non-BB air masses was similar in the two hours, both concentrated in the nearby regions in the east and southeast of the station. The calculated contact time also did not show significant differences, only 1.8% shorter for BB air masses than that for Non-BB air masses. These results suggest that the ground surface was not a major contributor. The elevated HONO concentrations observed during BB episodes were mainly due to aerosol-related heterogeneous processes.

3.2.2 Roles of BB aerosols on HONO chemistry

The surface area and chemical nature of aerosol particles are the two dominating factors that influence the aerosol-related heterogeneous processes to produce HONO. In this study, the enhanced aerosol particle loadings associated with the BB plumes (Figs. 1 and 3a), providing large aerosol surface areas (Fig. 6), should aid the NO_2 to HONO conversion. Besides the particle mass concentration, also the particle specific surface area related to the particle size distribution and morphology influences the total particle surface area concentration. In Fig. 8a, we present the relationship between the particle specific surface area (the concentration ratios of particle surface area to $PM_{2.5}$) and particle mass concentrations ($PM_{2.5}$). The specific surface areas were anti-correlated with the particle concentrations for Non-BB aerosols. However, the data points for BB samples were not on this fitting curve, but rather above it. These results suggest that the particle specific surface area was not an independent variable but was related to the particle mass concentration. Therefore, to compare the particle specific surface area concentrations, we selected the samples with the $PM_{2.5}$ mass in the overlap concentration range 100–150 μg m^{-3} during both BB and non-BB periods (Fig. 8a and 8b), and compared their surface area concentrations calculated by the size distribution (Fig. 8c). The results showed a significantly larger surface area concentration for BB aerosols compared with non-BB aerosols. This clearly suggests that BB aerosols have a larger specific surface area than non-BB aerosol, favoring NO_2 to HONO conversion at similar levels of the PM mass concentration. To further investigate influence of BB aerosols on the particle specific surface area, we plotted the ratios of particle surface area to $PM_{2.5}$ against the abundance of potassium in

256 $PM_{2.5}$ (Fig. 9) during BB periods. The result showed a positively linear correlation
257 between the two metrics, suggesting a significant enhancement of BB aerosols on the
258 particle specific area concentrations. Besides the surface area concentrations, the
259 chemical nature of aerosols, which control the NO_2 conversion efficiency, is also a
260 candidate to influence the transformation of NO_2 to HONO.

261 Given that the concentrations of particle surface area were much higher in BB periods
262 than those in Non-BB periods, one hypothesis that NO_2 conversion efficiency
263 (represented by the ratios between $HONO/NO_2$ and aerosol surface area) is
264 independent of the aerosol surface area, should be testified before comparing the NO_2
265 conversion efficiency directly. In Fig. 10a, we plotted the relationship of NO_2
266 conversion efficiency to the particle surface area concentrations during both BB and
267 Non-BB periods. The results did not show an independent, but rather an
268 anti-correlated relationship between the two metrics. The data points of BB samples
269 lay above the Non-BB samples, indicating a higher NO_2 conversion efficiency of BB
270 aerosols. To further verify this point, we calculated the ratio between $HONO/NO_2$ and
271 aerosol surface area in a narrow surface area concentration range, $1.5–2.2\times10^{-9}$ m^2
272 cm^{-3}, which overlaps measured surface area concentrations during both BB and
273 Non-BB periods (Fig. 10a). The values of this ratio were ~40% higher during the BB
274 period than that during Non-BB period (Fig. 10b), further suggesting the NO_2
275 conversion efficiency of BB aerosols was higher than that of Non-BB aerosols.

276 In summary, the elevated HONO formation observed in BB plumes was caused by the
277 combined effects of enhanced particle loadings, higher specific aerosol surface areas,
278 and more efficient conversion of NO_2 to HONO on particle surfaces. It is well known
279 that high particle loadings associated with BB are caused by both primary particle
280 emissions and secondary aerosol formation during the atmospheric transport (Andreae
281 and Merlet, 2001; Li et al., 2003; Capes et al., 2008). Large aerosol specific surface
282 areas are probably due to the extremely high number concentrations of accumulation
283 mode particles during BB (Janhäll et al., 2010), and possibly the irregular shape of
284 soot particles (Dobbins and Megaridis, 1987; Cai et al., 1993), which is one major

product of BB. The higher NO_2 to HONO conversion efficiency on particle surfaces in BB plumes compared with non-BB air is a complex issue. One possible reason is the high abundance of organic (e.g. humic like) substances and soot particles (Reid et al., 2005), which are high-performance medians to convert NO_2 to HONO. This is supported by the much higher concentrations of organics and black carbons, which were estimated as the differences of $PM_{2.5}$ and the water soluble ions, in BB periods than those in Non-BB periods (see Fig. 3b).

3.3 Influence of mixed plume of biomass burning and fossil fuel emissions on HONO chemistry

An intense BB episode mixed with FF emissions that significant influenced on the everyday weather was observed on 10 June, 2012 (from 18:00 on 9 June to 05:00 on 11 June) (Ding et al., 2013b). Interestingly, the highest mixing ratios of HONO, exceeding 5 ppbv, occurred during this episode (Fig. 1). The solar radiation intensity was significantly decreased in the daytime of this episode due to the extremely high particle loading (See Fig. 3 in Ding et al., 2013b), and HONO concentrations during the daytime were at a similar level as those during the nighttime. Again, we investigated the relation between HONO and potassium. The result showed poorly correlation (Fig. 11a), suggesting that the enhanced HONO concentrations during the case of 10 June were secondarily produced. Although a high particle loading should be a contributor to the high HONO levels, it was not likely the most predominant factor because the PM concentrations during this event were comparable to the peak concentrations during the other BB episodes (Fig. 1). Another possible reason is that the plumes on 10 June were more aged than the other BB plumes, which would enhance the HONO production with a longer NO_2 contact time with aerosol surface. Here, we deployed the ratio of nitrate to NO_y to estimate the atmospheric processing time. As shown in Fig. 11b and 11c, all the BB plumes were in the same regime (Fig. 10b), and the values were similar, suggesting that there were no significant differences of atmospheric processing time for both general BB plumes and 10 June case.

Figure 12 shows the scatter plot between HONO and NO_2 concentrations during the BB periods. The dataset was separated into two groups: the beginning stage of 10 June (red squares, the first 5 hours, 18:00-22:00, on 9 June) combined with other BB episodes (blue squares) and later stage of the 10 June case (green circle dots). Both groups revealed a strong relation between HONO and NO_2 with a correlation coefficient higher than 0.8. The slope of the regression of the latter stage of the 10 June case was almost a factor of 2 higher (0.12) than that for the other group (0.07, mostly the data points of other BB episodes), indicating a higher NO_2 to HONO conversion potential of the aerosols in the later stage of the 10 June case compared with other BB episodes.

To further verify this point and exclude the influence of particle loading, samples with $PM_{2.5}$ concentrations in range of 190–300 μg m^{-3} (the overlapping parts) were selected from both these groups. Although the selected samples had similar PM concentration levels (Fig. 13a), the HONO/NO_2 ratios (Fig. 13b) and ratios between HONO/NO_2 and $PM_{2.5}$ (Fig. 13c) were much higher on 10 June than during the other BB episodes, indicating a higher potential for the aerosols on 10 June to convert NO_2 to HONO. It should be noted that particle surface area data were not available for the 10 June case because the extremely high particle loading influenced the sample inlet of the DMPS. The exact contributors to the enhancement of NO_2 conversion potentials, which was either higher specific aerosol surface areas or stronger conversion efficiency, are therefore not clear.

Our previous study demonstrated that the episode on 10 June was caused not only by BB but a mixture of intense BB and anthropogenic FF emissions (Ding et al., 2013b). As shown in Fig. 14, the SO_2 concentration was low at the beginning stage of this episode and then gradually increased, suggesting the mixing of anthropogenic pollutions rich in SO_2 with the BB particles several hours after the invasion of the BB plume. This is why the chemical features (HONO/NO_2) in the plume of the beginning stage of the 10 June case was similar to that in other BB episodes, yet very different from the later stage of the 10 June case (Fig. 12).

The mix of BB plumes and FF emissions will promote the formation of secondary aerosols (e. g. sulfate and secondary organic aerosols (SOA)) on BB particles, and thus modify their morphology and surface chemical nature (Li et al., 2003; Capes et al., 2008). As shown in Fig. 13d, the abundance of sulfate in $PM_{2.5}$ was significantly enhanced on 10 June case compared with other BB episodes. This coincided with the high NO_2 to HONO conversion efficiency (Fig. 13c), indicating a promotion of secondary aerosol formation on BB particles in the mixed plumes to produce HONO. To further verify this point, we plotted the nighttime HONO concentration against the sulfate concentration on 10 June (Fig. 15), noting that the daytime HONO chemistry is out of the scope of this work. The result shows a very good correlation between the two compounds (R=0.79), further suggesting the promotion of secondary aerosol formation on BB particles to HONO formation.

As discussed above, the specific surface area and chemical nature of aerosol particles are the key factors in determining their potential to convert NO_2 to HONO. Therefore, changes in the morphology and size distribution caused by secondary aerosol formation may have enhanced the specific surface area and led to increased HONO production in the mixed plumes. Another factor that might have enhanced HONO production could be the formation of some specific secondary material on BB particles, e.g. sulfate (Kleffmann et al., 1998) and secondary organic aerosols (Bröske et al., 2003). Finally, the enhanced RH aerosol water content (Fig. 14) caused by the production of hydrophilic species, e. g. sulfate, may also play a role in accelerating the NO_2 conversion (Stutz et al., 2004).

4. Conclusions

In this study, we analyzed a two-month measurement period of atmospheric HONO during the BB season of 2012 (May and June) at the SORPES central site in western YRD of eastern China, and demonstrated an important role of BB in the HONO chemistry in the ambient atmosphere. HONO formation was detected to be significantly elevated during the BB periods due to the combined effect of enhanced

particle loadings, larger specific surface areas of particles and higher NO_2 conversion efficiency on BB aerosols. An episode of mixed plumes of intense BB and anthropogenic FF emissions was observed on 10 June, during which the HONO production potentials from the conversion of NO_2 was further promoted by the formation of secondary particulate matter on BB particles.

Given that BB plumes are easily mixed with other anthropogenic pollutants in eastern China, their influences on the atmospheric chemistry is expected to be important via affecting the HONO budget and thus the radical pool. Furthermore, considering the potential re-activation of BB particles (e.g. soot) during their atmospheric transport, the HONO chemistry associated with BB plumes may affect atmospheric chemistry long distances downwind BB areas, even in the marine boundary layer. Therefore, more studies are encouraged on BB related chemistry in eastern China, which is a unique "laboratory" with frequent mixed plumes of BB and anthropogenic pollutions.

Acknowledgements

This work was funded by National Natural Science Foundation of China (D0512/0207131138 and D0510/41275129), the MOST 973 Program (2010CB428500), and the Jiangsu Provincial Science Fund for Distinguished Young Scholars (No. BK20140021). We thank T. Wang and L. Xue at The Hong Kong Polytechnic University for their suggestion on the data analysis. We are grateful of J. Kleffmann at Bergische Universität Wuppertal for his useful discussions on the data quality. We thank Metrohm Co. China for providing the MARGA analyzer and Z. Yan and J. Gao for their technical support for the instrument. We also thank the two anonymous referees for their construction and detailed comments during the open discussion of this manuscript (acpd-14-7859-2014).

References

Acker, K., and Möller, D.: Atmospheric variation of nitrous acid at different sites in Europe, Environmental Chemistry, 4, 242-255, http://dx.doi.org/10.1071/EN07023, 2007.

Alicke, B., Platt, U., and Stutz, J.: Impact of nitrous acid photolysis on the total hydroxyl radical budget during the Limitation of Oxidant Production/Pianura Padana Produzione di Ozono study in Milan, Journal of Geophysical Research: Atmospheres, 107, 8196, 10.1029/2000JD000075, 2002.

Ammann, M., Kalberer, M., Jost, D. T., Tobler, L., Rossler, E., Piguet, D., Gaggeler, H. W., and Baltensperger, U.: Heterogeneous production of nitrous acid on soot in polluted air masses, Nature, 395, 157-160, 1998.

Ammann, M., Rössler, E., Strekowski, R., and George, C.: Nitrogen dioxide multiphase chemistry: Uptake kinetics on aqueous solutions containing phenolic compounds, Phys Chem Chem Phys, 7, 2513-2518, 2005.

Andreae, M. O., and Merlet, P.: Emission of trace gases and aerosols from biomass burning, Global Biogeochemical Cycles, 15, 955-966, 10.1029/2000gb001382, 2001.

Appel, B. R., Winer, A. M., Tokiwa, Y., and Biermann, H. W.: Comparison of atmospheric nitrous acid measurements by annular denuder and differential optical absorption systems, Atmospheric Environment. Part A. General Topics, 24, 611-616, http://dx.doi.org/10.1016/0960-1686(90)90016-G, 1990.

Aubin, D. G., and Abbatt, J. P. D.: Interaction of NO2 with Hydrocarbon Soot: Focus on HONO Yield, Surface Modification, and Mechanism, The Journal of Physical Chemistry A, 111, 6263-6273, 10.1021/jp068884h, 2007.

Aumont, B., Madronich, S., Ammann, M., Kalberer, M., Baltensperger, U., Hauglustaine, D., and Brocheton, F.: On the NO2 + soot reaction in the atmosphere, Journal of Geophysical Research: Atmospheres, 104, 1729-1736, 10.1029/1998jd100023, 1999.

Barnes, I., and Rudziński, K. J.: Disposal of Dangerous Chemicals in Urban Areas and Mega Cities-Role of Oxides and Acids of Nitrogen in Atmospheric Chemistry, Springer, 2012.

Bedjanian, Y., and El Zein, A.: Interaction of NO2 with TiO2 Surface Under UV Irradiation: Products Study, The Journal of Physical Chemistry A, 116, 1758-1764, 10.1021/jp210078b, 2012.

Bröske, R., Kleffmann, J., and Wiesen, P.: Heterogeneous conversion of NO2 on secondary organic aerosol surfaces: A possible source of nitrous acid (HONO) in the atmosphere?, Atmos. Chem. Phys., 3, 469-474, 10.5194/acp-3-469-2003, 2003.

Burling, I. R., Yokelson, R. J., Griffith, D. W. T., Johnson, T. J., Veres, P., Roberts, J. M., Warneke, C., Urbanski, S. P., Reardon, J., Weise, D. R., Hao, W. M., and de Gouw, J.: Laboratory measurements of trace gas emissions from biomass burning of fuel types from the southeastern and southwestern United States, Atmos. Chem. Phys., 10, 11115-11130, 10.5194/acp-10-11115-2010, 2010.

Cai, J., Lu, N., and Sorensen, C. M.: Comparison of size and morphology of soot aggregates as determined by light scattering and electron microscope analysis, Langmuir, 9, 2861-2867, 10.1021/la00035a023, 1993.

Capes, G., Johnson, B., McFiggans, G., Williams, P. I., Haywood, J., and Coe, H.: Aging of biomass burning aerosols over West Africa: Aircraft measurements of chemical composition, microphysical properties, and emission ratios, Journal of Geophysical Research: Atmospheres, 113, D00C15, 10.1029/2008JD009845, 2008.

Ding, A., Wang, T., and Fu, C.: Transport characteristics and origins of carbon monoxide and ozone in Hong Kong, South China, Journal of Geophysical Research: Atmospheres, 118, 9475-9488, 10.1002/jgrd.50714, 2013a.

Ding, A. J., Fu, C. B., Yang, X. Q., Sun, J. N., Petäjä, T., Kerminen, V. M., Wang, T., Xie, Y., Herrmann, E., Zheng, L. F., Nie, W., Liu, Q., Wei, X. L., and Kulmala, M.: Intense atmospheric pollution modifies weather: a case of mixed biomass burning with fossil fuel combustion pollution in eastern China, Atmos. Chem. Phys., 13, 10545-10554, 10.5194/acp-13-10545-2013, 2013b.

Ding, A. J., Fu, C. B., Yang, X. Q., Sun, J. N., Zheng, L. F., Xie, Y. N., Herrmann, E., Nie, W., Petäjä, T., Kerminen, V. M., and Kulmala, M.: Ozone and fine particle in the western Yangtze River Delta: an overview of 1 yr data at the SORPES station, Atmos. Chem. Phys., 13, 5813-5830, 10.5194/acp-13-5813-2013, 2013c.

Dobbins, R., and Megaridis, C.: Morphology of flame-generated soot as determined by thermophoretic sampling, Langmuir, 3, 254-259, 1987.

Elshorbany, Y., Barnes, I., Becker, K. H., Kleffmann, J., and Wiesen, P.: Sources and cycling of tropospheric hydroxyl radicals—an overview, Int. J. Res. Phys. Chem. Chem. Phys, 2010.

Elshorbany, Y. F., Steil, B., Brühl, C., and Lelieveld, J.: Impact of HONO on global atmospheric chemistry calculated with an empirical parameterization in the EMAC model, Atmos. Chem. Phys., 12, 9977-10000, 10.5194/acp-12-9977-2012, 2012.

Elshorbany, Y. F., Crutzen, P. J., Steil, B., Pozzer, A., Tost, H., and Lelieveld, J.: Global and regional impacts of HONO on the chemical composition of clouds and aerosols, Atmos. Chem. Phys., 14, 1167-1184, 10.5194/acp-14-1167-2014, 2014.

Genfa, Z., Slanina, S., Brad Boring, C., Jongejan, P. A. C., and Dasgupta, P. K.: Continuous wet denuder measurements of atmospheric nitric and nitrous acids during the 1999 Atlanta Supersite, Atmospheric Environment, 37, 1351-1364, http://dx.doi.org/10.1016/S1352-2310(02)01011-7, 2003.

George, C., Strekowski, R. S., Kleffmann, J., Stemmler, K., and Ammann, M.: Photoenhanced uptake of gaseous NO2 on solid organic compounds: a photochemical source of HONO?, Faraday Discussions, 130, 195-210, 10.1039/b417888m, 2005.

Gonçalves, M., Dabdub, D., Chang, W. L., Jorba, O., and Baldasano, J. M.: Impact of HONO sources on the performance of mesoscale air quality models, Atmospheric Environment, 54, 168-176, http://dx.doi.org/10.1016/j.atmosenv.2012.02.079, 2012.

Harrison, R., and Collins, G.: Measurements of Reaction Coefficients of NO2 and HONO on Aerosol Particles, Journal of Atmospheric Chemistry, 30, 397-406, 10.1023/a:1006094304069, 1998.

Harrison, R. M., and Kitto, A.-M. N.: Evidence for a surface source of atmospheric nitrous acid, Atmospheric Environment, 28, 1089-1094, http://dx.doi.org/10.1016/1352-2310(94)90286-0, 1994.

Hofzumahaus, A., Rohrer, F., Lu, K., Bohn, B., Brauers, T., Chang, C.-C., Fuchs, H., Holland, F., Kita, K., Kondo, Y., Li, X., Lou, S., Shao, M., Zeng, L., Wahner, A., and Zhang, Y.: Amplified Trace Gas Removal in the Troposphere, Science, 324, 1702-1704, 10.1126/science.1164566, 2009.

Janhäll, S., Andreae, M. O., and Pöschl, U.: Biomass burning aerosol emissions from vegetation fires: particle number and mass emission factors and size distributions, Atmos. Chem. Phys., 10, 1427-1439, 10.5194/acp-10-1427-2010, 2010.

Kalberer, M., Ammann, M., Arens, F., Gäggeler, H. W., and Baltensperger, U.: Heterogeneous formation of nitrous acid (HONO) on soot aerosol particles, Journal of Geophysical Research: Atmospheres, 104, 13825-13832, 10.1029/1999jd900141, 1999.

Kleffmann, J., Becker, K. H., and Wiesen, P.: Heterogeneous NO2 conversion processes on acid surfaces: possible atmospheric implications, Atmospheric Environment, 32, 2721-2729, http://dx.doi.org/10.1016/S1352-2310(98)00065-X, 1998.

Kleffmann, J., H. Becker, K., Lackhoff, M., and Wiesen, P.: Heterogeneous conversion of NO2 on carbonaceous surfaces, Phys Chem Chem Phys, 1, 5443-5450, 10.1039/a905545b, 1999.

Kleffmann, J., Gavriloaiei, T., Hofzumahaus, A., Holland, F., Koppmann, R., Rupp, L., Schlosser, E., Siese, M., and Wahner, A.: Daytime formation of nitrous acid: A major source of OH radicals in a forest, Geophysical Research Letters, 32, L05818, 10.1029/2005GL022524, 2005.

Kleffmann, J., and Wiesen, P.: Heterogeneous conversion of NO2 and NO on HNO3 treated soot surfaces: atmospheric implications, Atmos. Chem. Phys., 5, 77-83, 10.5194/acp-5-77-2005, 2005.

Kleffmann, J.: Daytime Sources of Nitrous Acid (HONO) in the Atmospheric Boundary Layer, ChemPhysChem, 8, 1137-1144, 10.1002/cphc.200700016, 2007.

Kurtenbach, R., Becker, K. H., Gomes, J. A. G., Kleffmann, J., Lörzer, J. C., Spittler, M., Wiesen, P., Ackermann, R., Geyer, A., and Platt, U.: Investigations of emissions and heterogeneous formation of HONO in a road traffic tunnel, Atmospheric Environment, 35, 3385-3394, http://dx.doi.org/10.1016/S1352-2310(01)00138-8, 2001.

Langridge, J. M., Gustafsson, R. J., Griffiths, P. T., Cox, R. A., Lambert, R. M., and Jones, R. L.: Solar driven nitrous acid formation on building material surfaces containing titanium dioxide: A concern for air quality in urban areas?, Atmospheric Environment, 43, 5128-5131, http://dx.doi.org/10.1016/j.atmosenv.2009.06.046, 2009.

Li, G., Lei, W., Zavala, M., Volkamer, R., Dusanter, S., Stevens, P., and Molina, L. T.: Impacts of HONO sources on the photochemistry in Mexico City during the MCMA-2006/MILAGO Campaign, Atmos. Chem. Phys., 10, 6551-6567, 10.5194/acp-10-6551-2010, 2010.

Li, J., Pósfai, M., Hobbs, P. V., and Buseck, P. R.: Individual aerosol particles from biomass burning in southern Africa: 2, Compositions and aging of inorganic particles, Journal of Geophysical Research: Atmospheres, 108, 8484, 10.1029/2002JD002310, 2003.

Li, X., Brauers, T., Häseler, R., Bohn, B., Fuchs, H., Hofzumahaus, A., Holland, F., Lou, S., Lu, K. D., Rohrer, F., Hu, M., Zeng, L. M., Zhang, Y. H., Garland, R. M., Su, H., Nowak, A., Wiedensohler, A., Takegawa, N., Shao, M., and Wahner, A.: Exploring the atmospheric chemistry of nitrous acid (HONO) at a rural site in Southern China, Atmos. Chem. Phys., 12,

1497-1513, 10.5194/acp-12-1497-2012, 2012.

Longfellow, C. A., Ravishankara, A. R., and Hanson, D. R.: Reactive uptake on hydrocarbon soot: Focus on NO2, Journal of Geophysical Research: Atmospheres, 104, 13833-13840, 10.1029/1999jd900145, 1999.

Makkonen, U., Virkkula, A., Mäntykenttä, J., Hakola, H., Keronen, P., Vakkari, V., and Aalto, P. P.: Semi-continuous gas and inorganic aerosol measurements at a Finnish urban site: comparisons with filters, nitrogen in aerosol and gas phases, and aerosol acidity, Atmos. Chem. Phys., 12, 5617-5631, 10.5194/acp-12-5617-2012, 2012.

Monge, M. E., D'Anna, B., Mazri, L., Giroir-Fendler, A., Ammann, M., Donaldson, D. J., and George, C.: Light changes the atmospheric reactivity of soot, Proceedings of the National Academy of Sciences, 107, 6605-6609, 10.1073/pnas.0908341107, 2010.

Ndour, M., D'Anna, B., George, C., Ka, O., Balkanski, Y., Kleffmann, J., Stemmler, K., and Ammann, M.: Photoenhanced uptake of NO2 on mineral dust: Laboratory experiments and model simulations, Geophys. Res. Lett., 35, L05812, 10.1029/2007gl032006, 2008.

Nie, W., Wang, T., Xue, L. K., Ding, A. J., Wang, X. F., Gao, X. M., Xu, Z., Yu, Y. C., Yuan, C., Zhou, Z. S., Gao, R., Liu, X. H., Wang, Y., Fan, S. J., Poon, S., Zhang, Q. Z., and Wang, W. X.: Asian dust storm observed at a rural mountain site in southern China: chemical evolution and heterogeneous photochemistry, Atmos. Chem. Phys., 12, 11985-11995, 10.5194/acp-12-11985-2012, 2012.

Platt, U., Perner, D., Harris, G., Winer, A., and Pitts, J.: Observations of nitrous acid in an urban atmosphere by differential optical absorption, Nature, 285, 312- 314, doi:10.1038/285312a0, 1980.

Prince, A. P., Wade, J. L., Grassian, V. H., Kleiber, P. D., and Young, M. A.: Heterogeneous reactions of soot aerosols with nitrogen dioxide and nitric acid: atmospheric chamber and Knudsen cell studies, Atmospheric Environment, 36, 5729-5740, http://dx.doi.org/10.1016/S1352-2310(02)00626-X, 2002.

Reid, J. S., Koppmann, R., Eck, T. F., and Eleuterio, D. P.: A review of biomass burning emissions part II: intensive physical properties of biomass burning particles, Atmos. Chem. Phys., 5, 799-825, 10.5194/acp-5-799-2005, 2005.

Roberts, J. M., Veres, P., Warneke, C., Neuman, J. A., Washenfelder, R. A., Brown, S. S., Baasandorj, M., Burkholder, J. B., Burling, I. R., Johnson, T. J., Yokelson, R. J., and de Gouw, J.: Measurement of HONO, HNCO, and other inorganic acids by negative-ion proton-transfer chemical-ionization mass spectrometry (NI-PT-CIMS): application to biomass burning emissions, Atmos. Meas. Tech., 3, 981-990, 10.5194/amt-3-981-2010, 2010.

Sander, S. P., Golden, D., Kurylo, M., Moortgat, G., Wine, P., Ravishankara, A., Kolb, C., Molina, M., Finlayson-Pitts, B., and Huie, R.: Chemical kinetics and photochemical data for use in atmospheric studies evaluation number 15, 2006.

Sorgel, M., Regelin, E., Bozem, H., Diesch, J. M., Drewnick, F., Fischer, H., Harder, H., Held, A., Hosaynali-Beygi, Z., and Martinez, M.: Quantification of the unknown HONO daytime source and its relation to NO2, Atmospheric Chemistry & Physics Discussions, 11, 15119-15155, 2011.

Spindler, G., Hesper, J., Brüggemann, E., Dubois, R., Müller, T., and Herrmann, H.: Wet annular

denuder measurements of nitrous acid: laboratory study of the artefact reaction of NO2 with S(IV) in aqueous solution and comparison with field measurements, Atmospheric Environment, 37, 2643-2662, http://dx.doi.org/10.1016/S1352-2310(03)00209-7, 2003.

Stemmler, K., Ammann, M., Donders, C., Kleffmann, J., and George, C.: Photosensitized reduction of nitrogen dioxide on humic acid as a source of nitrous acid, Nature, 440, 195-198, 2006.

Stutz, J., Alicke, B., and Neftel, A.: Nitrous acid formation in the urban atmosphere: Gradient measurements of NO2 and HONO over grass in Milan, Italy, J. Geophys. Res, 107, 2002.

Stutz, J., Alicke, B., Ackermann, R., Geyer, A., Wang, S., White, A. B., Williams, E. J., Spicer, C. W., and Fast, J. D.: Relative humidity dependence of HONO chemistry in urban areas, Journal of Geophysical Research: Atmospheres, 109, D03307, 10.1029/2003JD004135, 2004.

Su, H.: HONO: a Study to its Sources and Impacts from Field Measurements at the Sub-urban Areas of PRD Region, PhD Thesis of Peking University, 2008.

Su, H., Cheng, Y. F., Shao, M., Gao, D. F., Yu, Z. Y., Zeng, L. M., Slanina, J., Zhang, Y. H., and Wiedensohler, A.: Nitrous acid (HONO) and its daytime sources at a rural site during the 2004 PRIDE-PRD experiment in China, Journal of Geophysical Research: Atmospheres, 113, D14312, 10.1029/2007jd009060, 2008.

Su, H., Cheng, Y., Oswald, R., Behrendt, T., Trebs, I., Meixner, F. X., Andreae, M. O., Cheng, P., Zhang, Y., and Pöschl, U.: Soil Nitrite as a Source of Atmospheric HONO and OH Radicals, Science, 333, 1616-1618, 10.1126/science.1207687, 2011.

Th. Muller, R. D., G Spindler, E Bruggemann, R. Ackermann, A. Geyer, U. Platf: Measurements of Nitrous Acid by DOAS and Diffusion Denuders: A Comparison, Transactions on Ecology and the Environment, 28, ISSN 1743-3541, 1999.

VandenBoer, T. C., Brown, S. S., Murphy, J. G., Keene, W. C., Young, C. J., Pszenny, A. A. P., Kim, S., Warneke, C., de Gouw, J. A., Maben, J. R., Wagner, N. L., Riedel, T. P., Thornton, J. A., Wolfe, D. E., Dubé, W. P., Öztürk, F., Brock, C. A., Grossberg, N., Lefer, B., Lerner, B., Middlebrook, A. M., and Roberts, J. M.: Understanding the role of the ground surface in HONO vertical structure: High resolution vertical profiles during NACHTT-11, Journal of Geophysical Research: Atmospheres, 118, 10,155-110,171, 10.1002/jgrd.50721, 2013.

Veres, P., Roberts, J. M., Burling, I. R., Warneke, C., de Gouw, J., and Yokelson, R. J.: Measurements of gas-phase inorganic and organic acids from biomass fires by negative-ion proton-transfer chemical-ionization mass spectrometry, Journal of Geophysical Research: Atmospheres, 115, D23302, 10.1029/2010jd014033, 2010.

Wang, S., Zhou, R., Zhao, H., Wang, Z., Chen, L., and Zhou, B.: Long-term observation of atmospheric nitrous acid (HONO) and its implication to local NO2 levels in Shanghai, China, Atmospheric Environment, 77, 718-724, http://dx.doi.org/10.1016/j.atmosenv.2013.05.071, 2013.

Wong, K. W., Oh, H. J., Lefer, B. L., Rappenglück, B., and Stutz, J.: Vertical profiles of nitrous acid in the nocturnal urban atmosphere of Houston, TX, Atmos. Chem. Phys., 11, 3595-3609, 10.5194/acp-11-3595-2011, 2011.

Xu, Z., Wang, T., Xue, L. K., Louie, P. K. K., Luk, C. W. Y., Gao, J., Wang, S. L., Chai, F. H.,

605 and Wang, W. X.: Evaluating the uncertainties of thermal catalytic conversion in measuring
606 atmospheric nitrogen dioxide at four differently polluted sites in China, Atmospheric
607 Environment, 76, 221-226, http://dx.doi.org/10.1016/j.atmosenv.2012.09.043, 2013.

Figure Captions:

Fig. 1 Temporal variation of the concentrations of HONO, NO_2 $PM_{2.5}$ mass and potassium, at the SORPES central site during April to June 2009

Fig. 2 Whisker plot of diurnal variation of (a) HONO and (b) HONO/NO_2 at the SORPES central site during April to June 2012

Fig. 3 Comparisons of (a) $PM_{2.5}$ concentrations, (b) concentrations of organic matters in $PM_{2.5}$ (estimated by $PM_{2.5}$-WSIs), (c) NO_2 concentrations, (d) HONO concentrations, (e) HONO to NO_2 ratio and (f) HONO to NO_x ratio between biomass burning period and non-biomass burning period

Fig. 4 Map of 24-hr Lagrangian backward retroplume (100 m footprint layer) for biomass burning air masses (defined as K+/PM>2% or K+ >2 ug/m3) and active fire (pink dots) during 15 April - 25 June, 2012 (Data obtained from FIRMS MODIS Fire Archive)

Fig. 5 Scatter plot between the HONO and potassium concentration during biomass burning periods

Fig.6 Scatter plot between the HONO and NO_2 concentration during the BB periods (without the case on 10 June, red circles) and non-BB periods (blue triangles) with the particle surface area concentrations (6–800 nm) as the color scale

Fig. 7 Map showing the mean 2-hr backward residence time of air masses at the ground surface during (a) BB periods and (b) Non-BB periods.

Fig. 8 (a) Scatter plot between the ratio of particle surface area to $PM_{2.5}$ and $PM_{2.5}$ for nighttime samples during BB and Non-BB periods, (b) Whisker plot of $PM_{2.5}$ in the selected mass concentration range (100–150μg m^{-3}, showed in Fig. 7a) during BB (51 samples) and Non-BB period (27 samples), and (c) particle surface area size distributions for the same subsets of data

Fig. 9 Scatter plot between the ratio of particle surface area to $PM_{2.5}$ and the

abundance of potassium in $PM_{2.5}$ for nighttime samples during BB during BB period.

Fig. 10 (a) Scatter plot between ratios of $HONO/NO_2$ to particle surface area and particle surface area for nighttime samples during BB and Non-BB periods, (b) whisker plot of the ratios between $HONO/NO_2$ and particle surface area concentration in the selected particle surface area range ($1.5–2.2 \times 10^{-9}$ m^2 cm^{-3}) during the BB and non-BB periods

Fig. 11 (a) Scatter plot between the HONO and potassium concentration during the case of 10th June, (b) scatter plot between $PM_{2.5}$ nitrate and NO_y concentrations during BB periods (without the case of 10th June, blue solid squares) and the case of 10th June (green dots), (c) whisker plot of the ratios between nitrate and NOy during BB plume and mix plume (10th June).

Fig. 12 Scatter plot between HONO and NO_2 concentration during the BB periods (without the case of 10th June, blue solid squares), the beginning (red solid diamonds) and latter (green dots) state of the June 10thepisode

Fig. 13 Whisker plots of (a) $PM_{2.5}$ mass, (b) ratios of HONO to NO_2, (c) ratios of $HONO/NO_2$ to $PM_{2.5}$ mass, (d) ratios of sulfate to $PM_{2.5}$, in the selected $PM_{2.5}$ mass concentration range (190–300 μg m^{-3}) in BB plume (10 samples) and the mixed plume (27 samples)

Fig. 14 Temporal variations of HONO, $HONO/NO_2$ ratios, RH, $PM_{2.5}$, sulfate in $PM_{2.5}$ and SO_2 during 9 - 11 June 2012 at the SORPES central site

Fig. 15 Scatter plot between HONO and sulfate concentration in $PM_{2.5}$ during the nighttime on 10 June

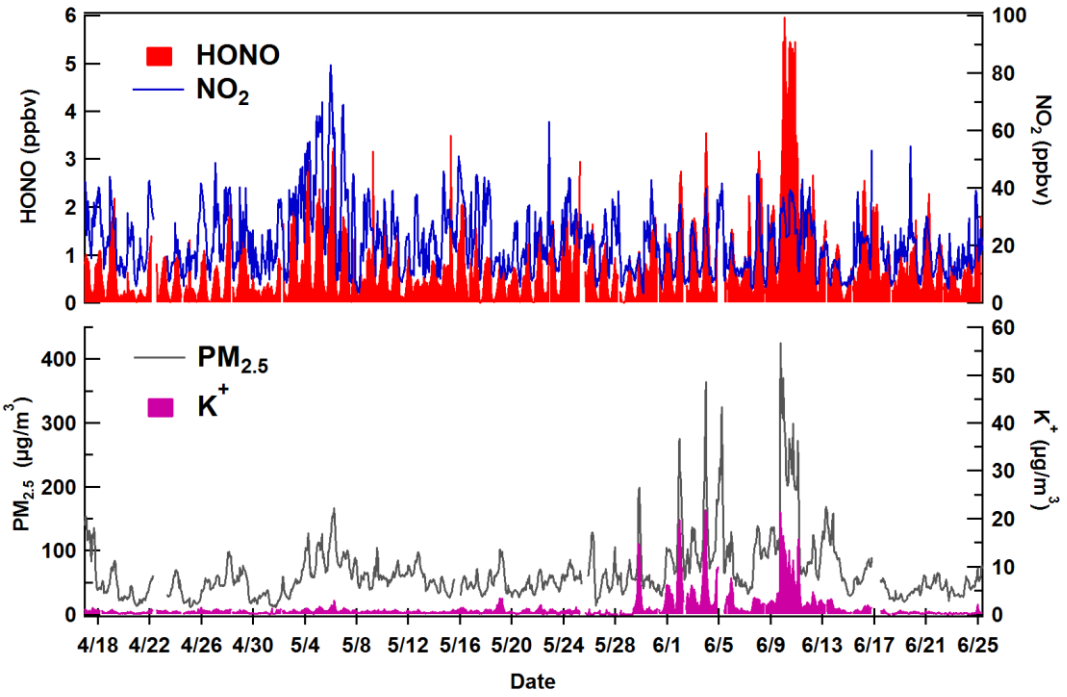

Fig. 1 Temporal variation of the concentrations of HONO, NO_2, $PM_{2.5}$ mass and potassium, at the SORPES central site during April to June 2009.

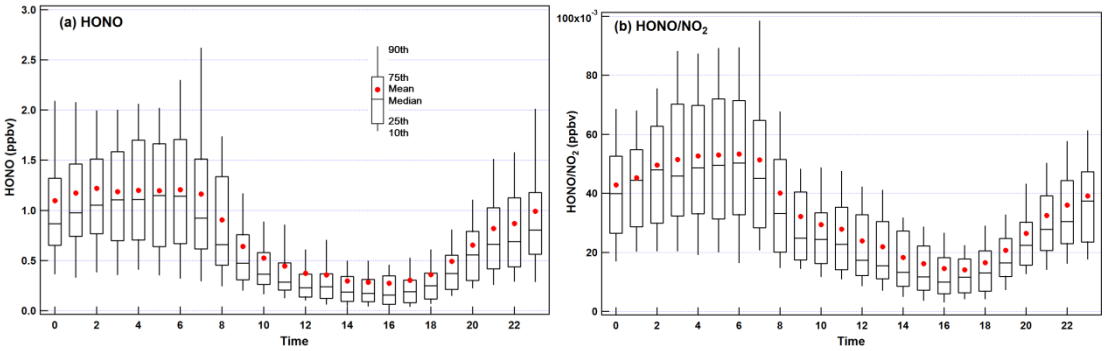

Fig. 2 Whisker plot of diurnal variation of (a) HONO and (b) $HONO/NO_2$ at the SORPES central site during April to June 2012.

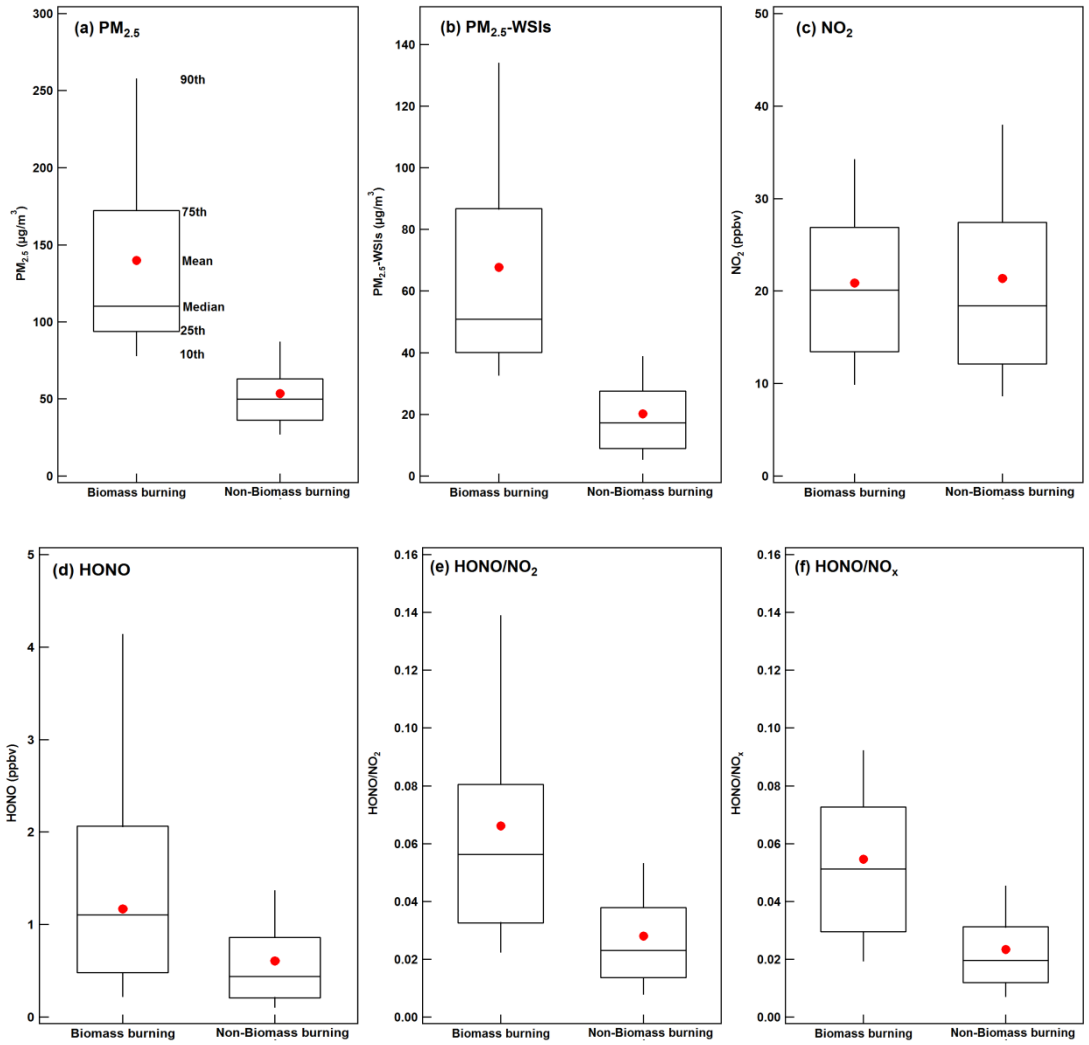

Fig. 3 Comparisons of (a) $PM_{2.5}$ concentrations, (b) concentrations of organic matters in $PM_{2.5}$ (estimated by $PM_{2.5}$-WSIs), (c) NO_2 concentrations, (d) HONO concentrations, (e) HONO to NO_2 ratio and (f) HONO to NO_x ratio between biomass burning period and non-biomass burning period.

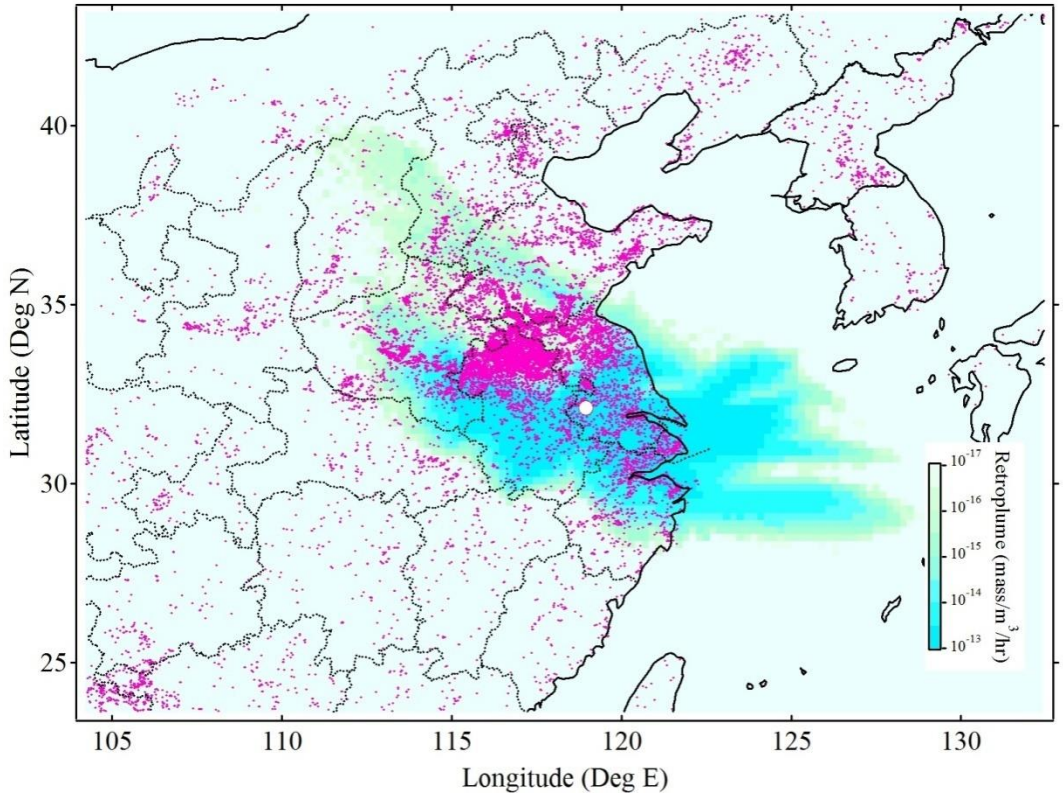

Fig. 4 Map of 24-hr Lagrangian backward retroplume (100 m footprint layer) for biomass burning air masses (defined as K^+ >2 ug m^{-3} and K^+/PM>2%) and active fire (pink dots) during 15 April - 25 June, 2012 (Data obtained from FIRMS MODIS Fire Archive).

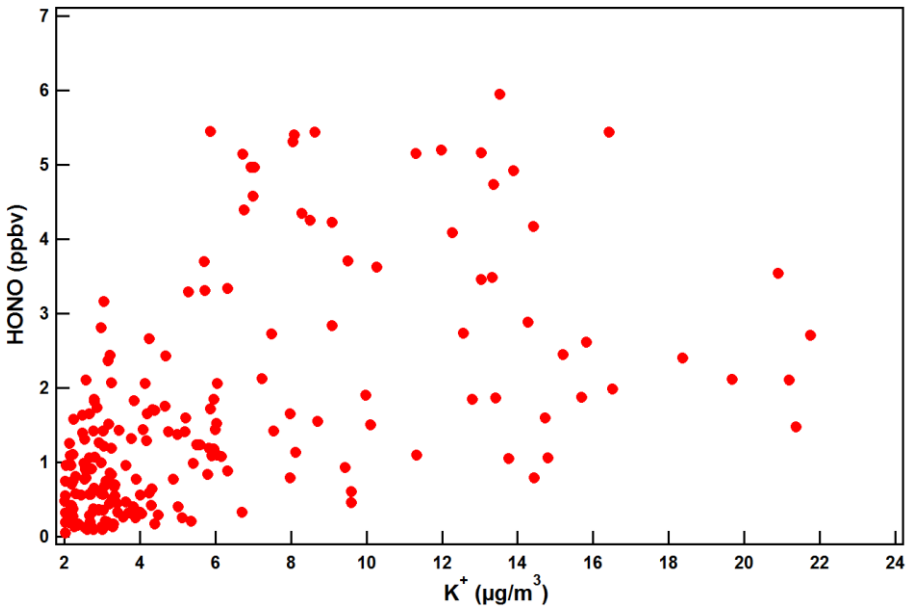

Fig. 5 Scatter plot between the HONO and potassium concentration during biomass burning periods.

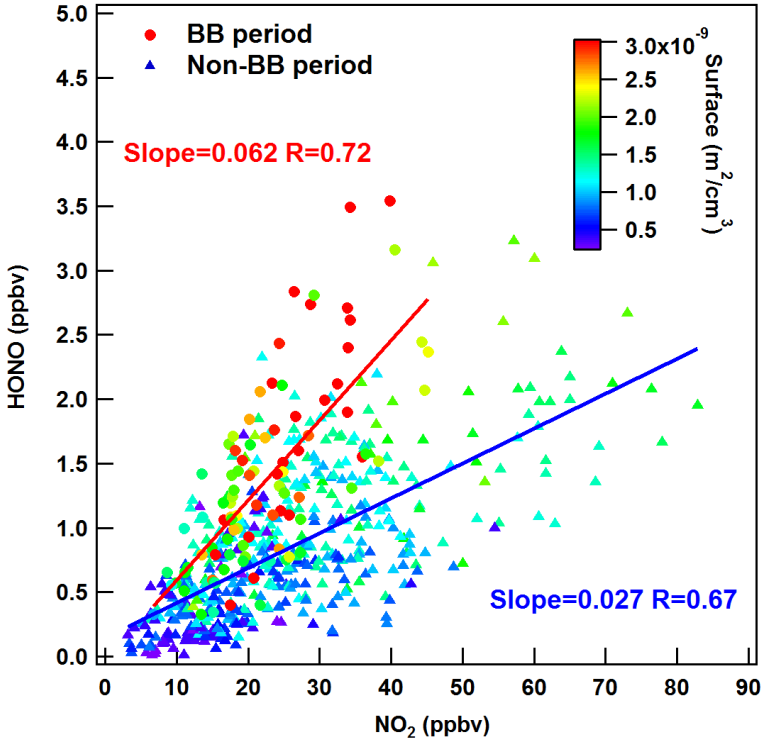

Fig.6 Scatter plot between the HONO and NO_2 concentration during the BB periods (without the case on 10 June, red circles) and non-BB periods (blue triangles) with the particle surface area concentrations (6–800 nm) as the color scale.

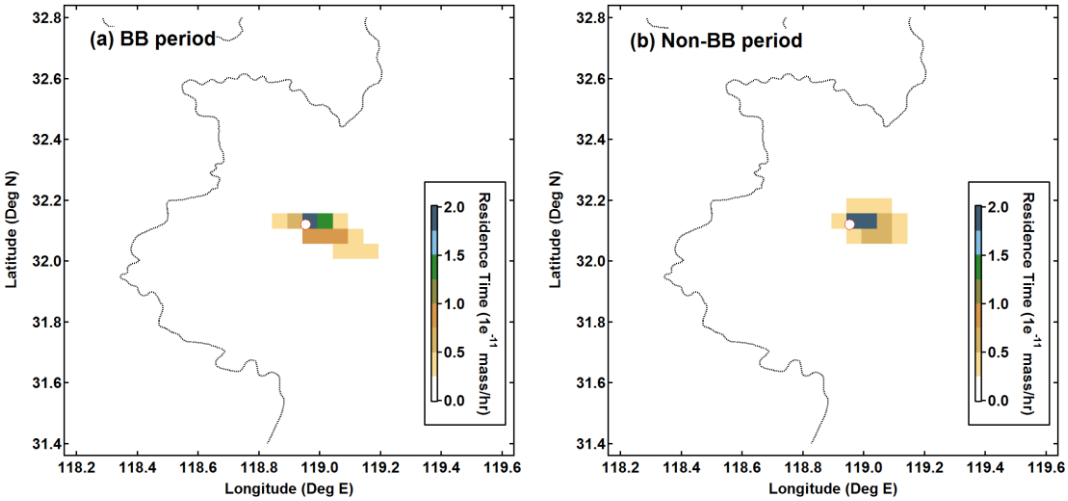

Fig. 7 Map showing the mean 2-hr backward residence time of air masses at the ground surface during (a) BB periods and (b) Non-BB periods

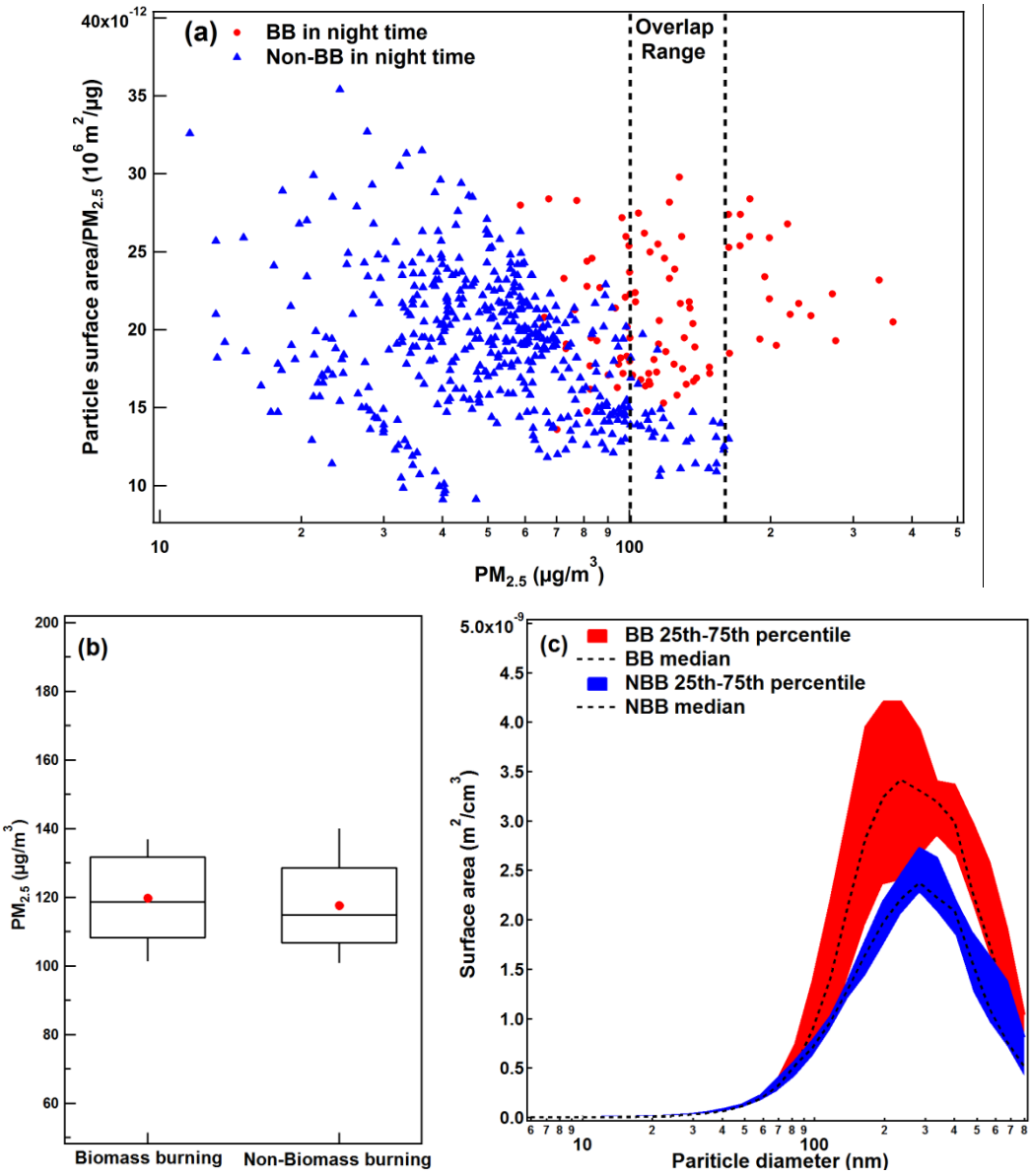

Fig. 8 (a) Scatter plot between the ratio of particle surface area to $PM_{2.5}$ and $PM_{2.5}$ for nighttime samples during BB and Non-BB periods, (b) Whisker plot of $PM_{2.5}$ in the selected mass concentration range (100–150µg m^{-3}, showed in Fig. 7a) during BB (51 samples) and Non-BB period (27 samples), and (c) particle surface area size distributions for the same subsets of data.

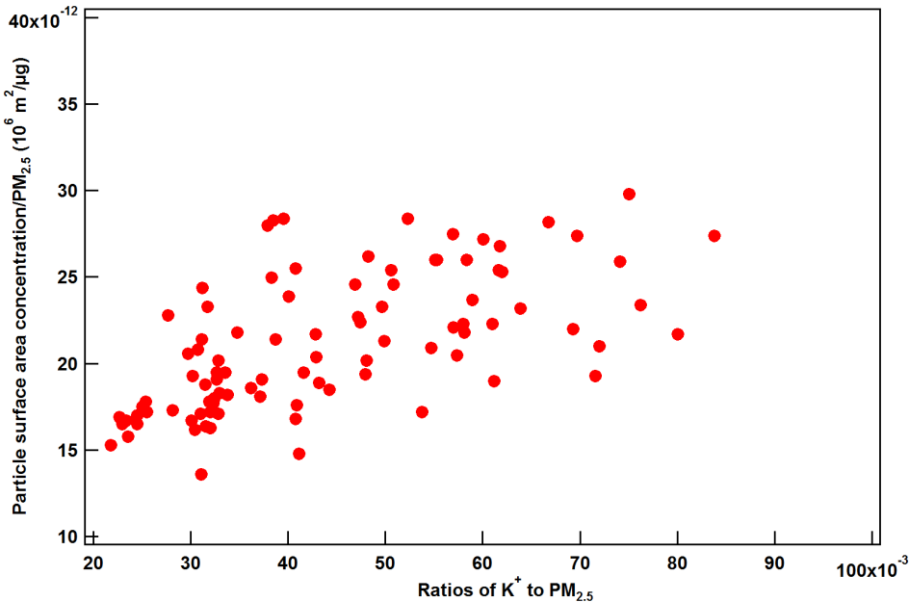

Fig. 9 Scatter plot between the ratio of particle surface area to $PM_{2.5}$ and the abundance of potassium in $PM_{2.5}$ for nighttime samples during BB during BB period.

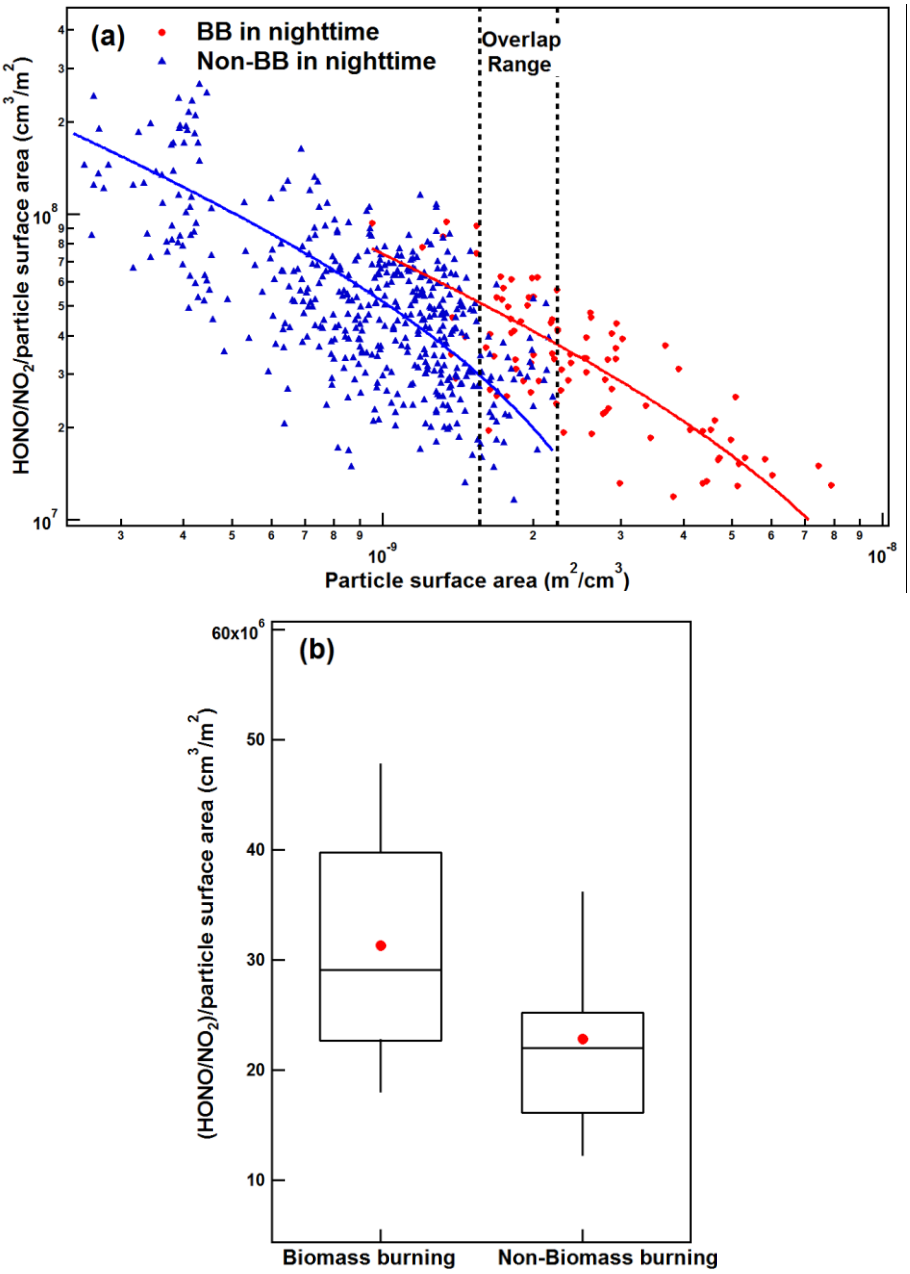

Fig. 10 (a) Scatter plot between ratios of $HONO/NO_2$ to particle surface area and particle surface area for nighttime samples during BB and Non-BB periods, (b) whisker plot of the ratios between $HONO/NO_2$ and particle surface area concentration in the selected particle surface area range ($1.5–2.2\times10^{-9}$ m^2 cm^{-3}) during the BB (35 samples) and non-BB periods (51 samples).

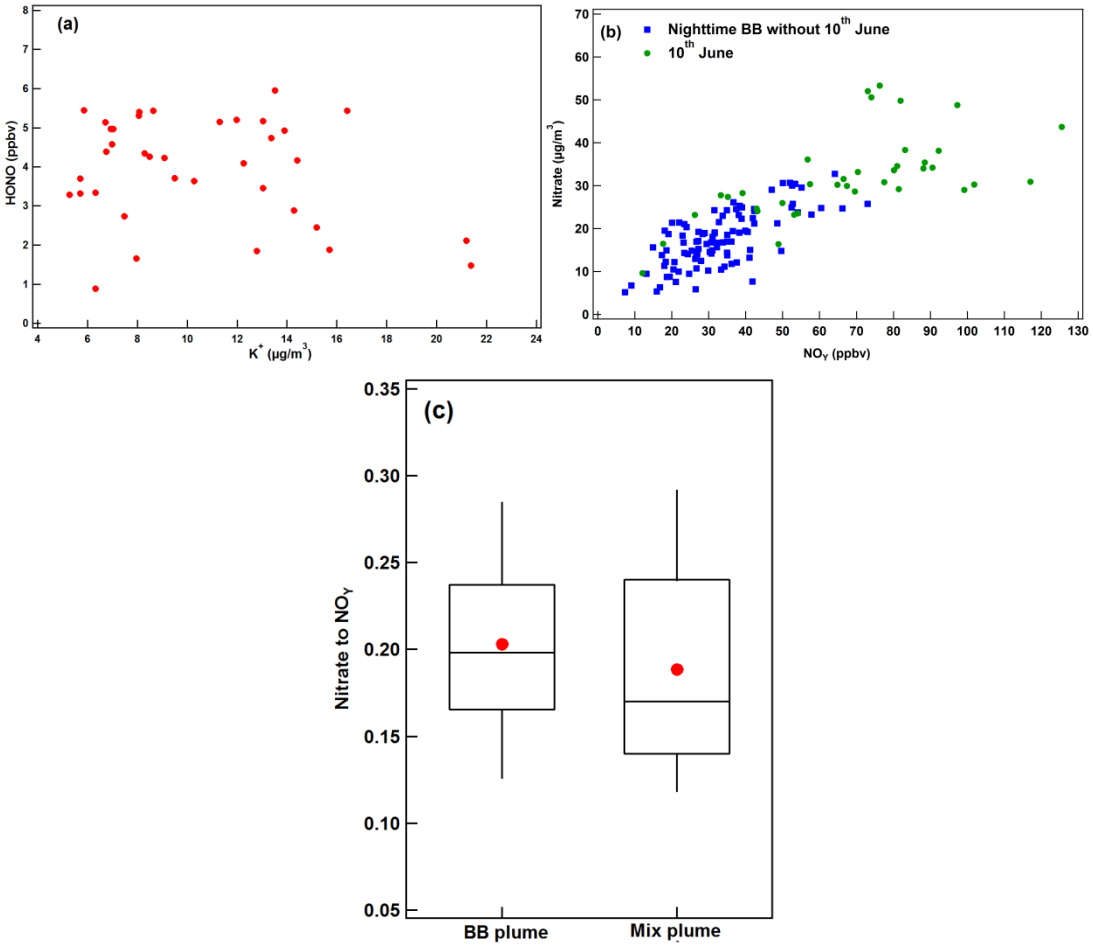

Fig. 11 (a) Scatter plot between the HONO and potassium concentration during the case of 10th June, (b) scatter plot between $PM_{2.5}$ nitrate and NO_y concentrations during BB periods (without the case of 10th June, blue solid squares) and the case of 10th June (green dots), (c) whisker plot of the ratios between nitrate and NOy during BB plume and mix plume (10th June).

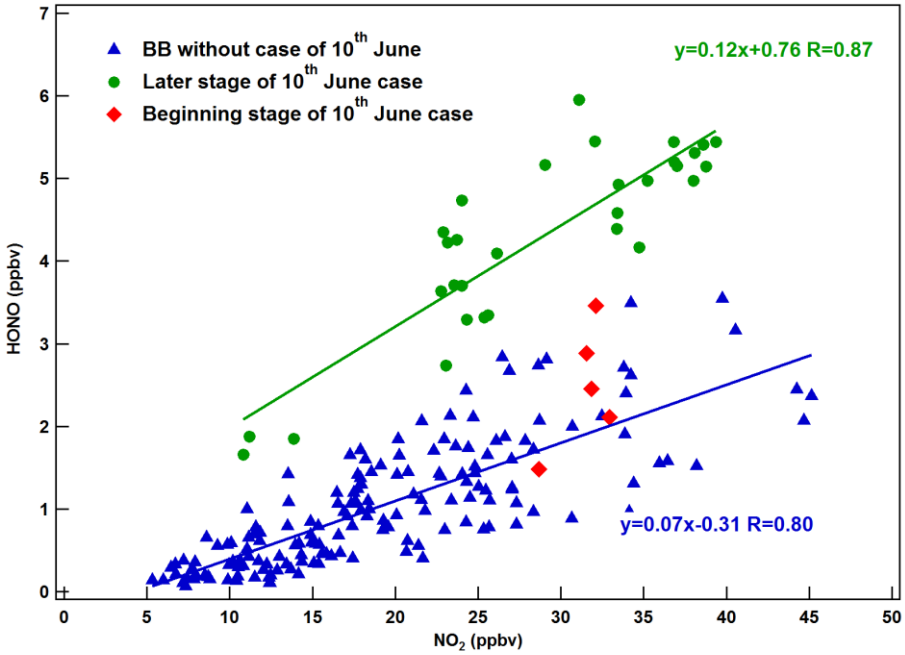

Fig. 12 Scatter plot between HONO and NO_2 concentration during the BB periods (without the case of 10th June, blue solid squares), the beginning (red solid diamonds) and latter (green dots) state of the June 10th episode.

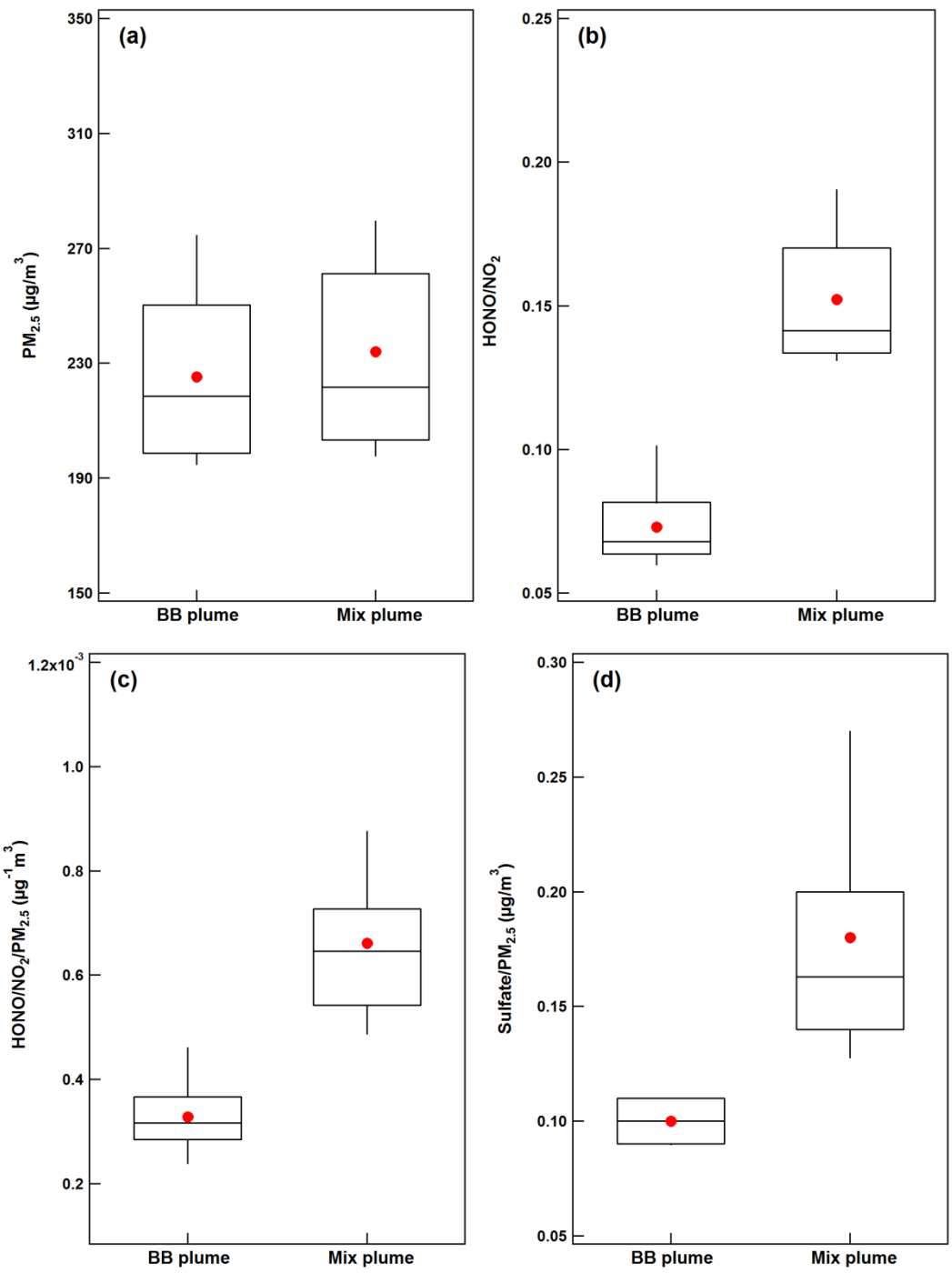

Fig. 13 Whisker plots of (a) $PM_{2.5}$ mass, (b) ratios of HONO to NO_2, (c) ratios of $HONO/NO_2$ to $PM_{2.5}$ mass, (d) ratios of sulfate to $PM_{2.5}$, in the selected $PM_{2.5}$ mass concentration range (190–300 μg m^{-3}) in BB plume (10 samples) and the mixed plume (27 samples).

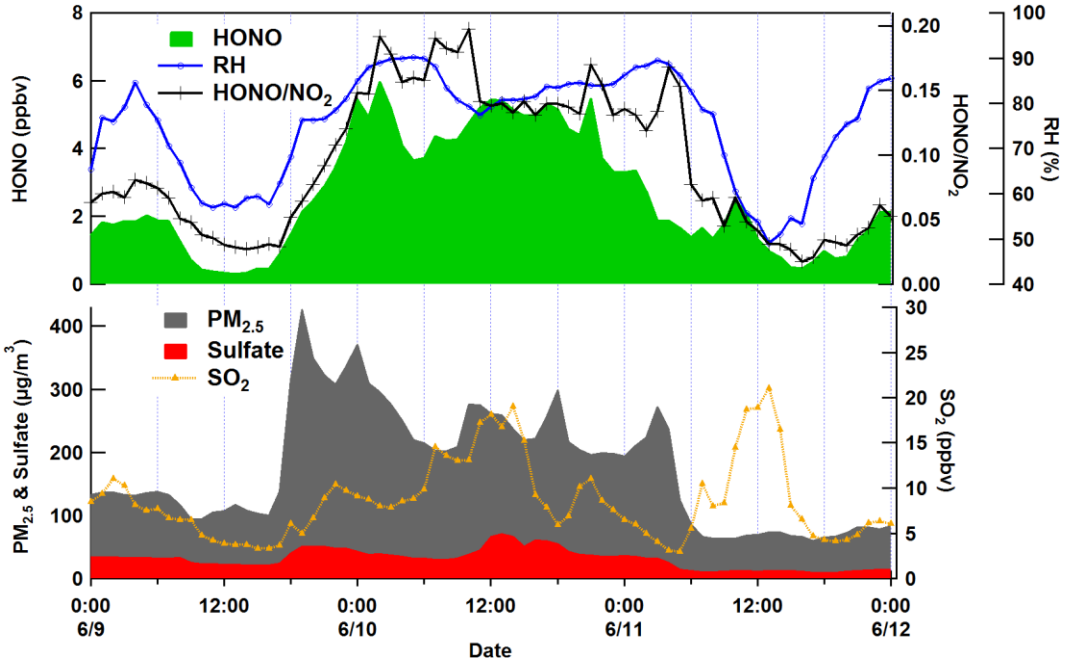

Fig. 14 Temporal variations of HONO, $HONO/NO_2$ ratios, RH, $PM_{2.5}$, sulfate in $PM_{2.5}$ and SO_2 during 9 - 11 June 2012 at the SORPES central site.

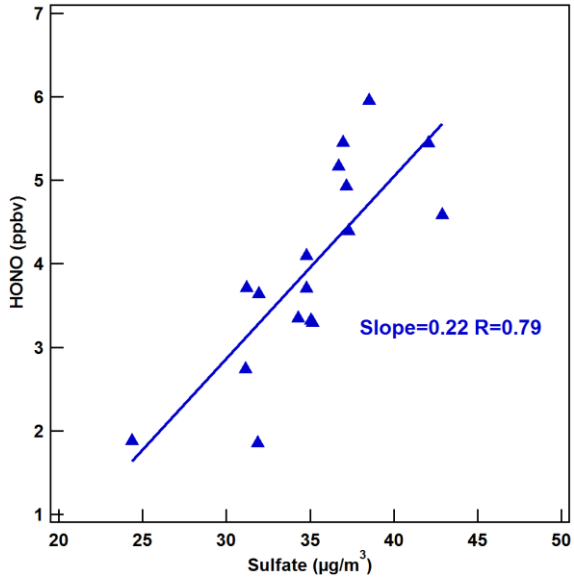

Fig. 15 Scatter plot between HONO and sulfate concentration in $PM_{2.5}$ during the nighttime on 10 June